

Perpendicular Subcritical Shock Structure in a Collisional Plasma Experiment

D. R. Russell^{1,*}, G. C. Burdiak², J. J. Carroll-Nellenback³, J. W. D. Halliday¹, J. D. Hare⁴, S. Merlini¹,
L. G. Suttle¹, V. Valenzuela-Villaseca¹, S. J. Eardley¹, J. A. Fullalove¹, G. C. Rowland¹, R. A. Smith¹,

A. Frank³, P. Hartigan⁵, A. L. Velikovich⁶, J. P. Chittenden¹ and S. V. Lebedev¹

¹*Blackett Laboratory, Imperial College London, London SW7 2AZ, United Kingdom*


²*First Light Fusion Ltd, Yarnton, Kidlington OX5 1QU, United Kingdom*

³*Department of Physics and Astronomy, University of Rochester, Rochester, New York 14627, USA*

⁴*Plasma Science and Fusion Center, Massachusetts Institute of Technology, Cambridge, Massachusetts 02139, USA*

⁵*Department of Physics and Astronomy, Rice University, Houston, Texas 77005-1892, USA*

⁶*Plasma Physics Division, U.S. Naval Research Laboratory, Washington, DC 20375, USA*

 (Received 19 January 2022; revised 14 October 2022; accepted 25 October 2022; published 22 November 2022)

We present a study of perpendicular subcritical shocks in a collisional laboratory plasma. Shocks are produced by placing obstacles into the supermagnetosonic outflow from an inverse wire array z pinch. We demonstrate the existence of subcritical shocks in this regime and find that secondary shocks form in the downstream. Detailed measurements of the subcritical shock structure confirm the absence of a hydrodynamic jump. We calculate the classical (Spitzer) resistive diffusion length and show that it is approximately equal to the shock width. We measure little heating across the shock ($< 10\%$ of the ion kinetic energy) which is consistent with an absence of viscous dissipation.

DOI: [10.1103/PhysRevLett.129.225001](https://doi.org/10.1103/PhysRevLett.129.225001)

Shock waves are ubiquitous in astrophysical [1], space, and laboratory plasmas and often include an embedded, dynamically significant magnetic field. The theoretical understanding of magnetohydrodynamic (MHD) shock waves was first established in the 1950s [2–5]. In particular, it was discovered that resistive Ohmic heating, a dissipation mechanism specific to MHD, can shape shock structures. Since resistivity does not directly dissipate the plasma kinetic energy, there is a critical value of the upstream magnetosonic Mach number, M_C , indicating the maximum strength of MHD shocks shaped by Ohmic heating alone. Subcritical shocks (with $M_{MS} < M_C$) have a supersonic, $M_{S,d} > 1$, but submagnetosonic, $M_{MS,d} < 1$, downstream flow [6,7] and are predicted to have a shock width equal to the resistive diffusion length. The absence of viscous dissipation in subcritical shocks also led to the prediction that hydrodynamic parameters should be continuous across the shock (with no mfp scale jump). In the astrophysical literature, subcritical MHD shocks in weakly ionized, low-density plasmas are labeled continuous (C) shocks [8,9]. The energy dissipation mechanism in C shocks is different from that discussed here, but the critical condition is the same.

Since then, studies of subcritical shocks have focused on the collisionless regime [10,11], motivated by the ubiquity of collisionless shocks in space and astrophysical plasmas. In these cases, the physical processes which generate entropy at the shock are more complicated than the collisional transport models [12–17]. This leads to difficulty in

defining the critical Mach number (due to the lack of downstream thermodynamic equilibrium) and determining the plasma resistivity. Recent progress in magnetoinertial fusion [18–22], has stimulated renewed interest in MHD shocks propagating through dense, collision-dominated plasmas [23]. In particular, recent experiments studying the implosion of magnetized inertial confinement fusion capsules have shown an increased yield and anisotropic shock structure [24–26]. The structures of MHD shocks in this regime have been investigated theoretically [27,28] but never measured experimentally.

Since $M_S > 1$ downstream of a subcritical shock, what would the overall shock structure look like if the downstream were disturbed? Theory suggests that hydrodynamic shocks could form on a scale smaller than the resistive diffusion length. In contrast to subcritical shocks, these would feature viscous ion heating, and observation of this would be important for interpreting observations of astrophysical shocks where the shock structure is typically not resolved.

This Letter reports the first experimental study of subcritical shock structure in a highly collisional plasma (mfp \ll shock width). A supersonic ($M_S \sim 2.5$), super-Alfvénic ($M_A \sim 3$), supermagnetosonic ($M_{MS} \sim 1.9$) plasma flow was produced by the current driven ablation of an inverse wire array z pinch [29], and shocks were studied by placing stationary obstacles into this flow [30]. The orientation of the obstacles produced perpendicular shocks, in which the advected magnetic field was perpendicular to the shock normal. Subcritical shocks were

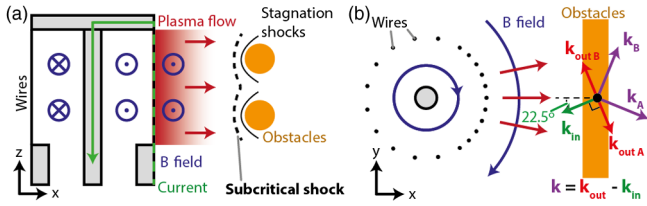


FIG. 1. Cross sectional diagram of the wire array and obstacles. (a) Side-on view. Cylindrical obstacles extend into the page, and shocks are indicated where they form in the experiment. (b) End-on view showing the azimuthal configuration of wires in the array and the vector diagram for the Thomson scattering diagnostic.

observed in which the downstream flow is shown to be supersonic. These measurements of a subcritical shock in a collisional plasma are the first of their kind and confirm the absence of a hydrodynamic jump as predicted by theory (e.g., [6,7,28]). Furthermore, detailed laser probing measurements allow the calculation of the resistive diffusion length L_η (using classical Spitzer resistivity) which we show to be equal to the shock width. The shock structure can therefore be described by classical resistive MHD, without the inclusion of anomalous resistivity. Finally, we observe secondary shocks in the downstream which are separate from the subcritical shock and for which the relevant Mach number is M_S .

The experimental setup is shown in Fig. 1. The inverse wire array z pinch was driven by the MAGPIE pulsed power generator (1.4 MA peak current, 240 ns rise time) [31]. A cylindrical arrangement (21 mm high and 20 mm in diameter) of 21 aluminium wires (each with a 40 μm diameter) surrounded a central cathode. This experimental geometry provided a $J \times B$ force which acted radially outward, accelerating the plasma ablated by the wires for the duration of the drive current [32]. Since some of the drive current passed through the ablated plasma surrounding each wire, a fraction of the magnetic field was advected by the flow [33]. The 11 wires closest to the obstacles had an angular separation of 11.25° while the remaining wires had an angular separation of 22.5°; see Fig. 1(b). The smaller wire separation reduced azimuthal density variation by reducing the divergence of the flow and allowing outflows from adjacent wires to merge [30].

Two 4 mm diameter cylindrical brass obstacles were placed 10 mm from the ablating wires and were oriented with their axes parallel to the advected magnetic field (Fig. 1). The obstacles had a center-to-center separation of 9 mm in the vertical, z , direction and were 40 mm in length. The obstacles reproducibly (> 15 shots) produced shocks in the plasma flow which were extended in the y direction and approximately stationary in the laboratory frame for ~ 200 ns (many hydrodynamic crossing times). The shocks formed due to magnetic field and plasma pileup in front of the obstacle surface as the aluminium plasma collided with the solid obstacles.

The plasma was studied with a number of diagnostics. Electron density was measured with laser interferometry

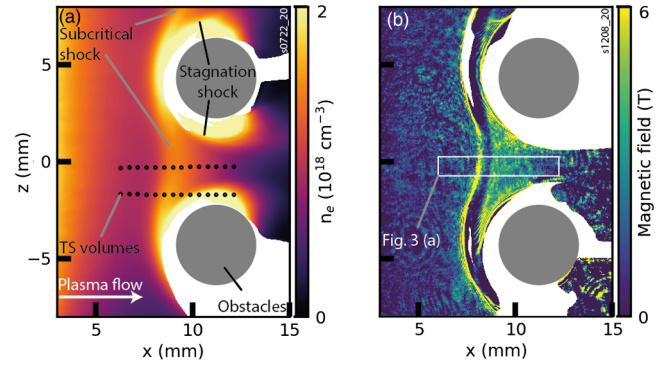


FIG. 2. Electron density and magnetic field measurements. (a) Electron density recorded 426 ns after current start. The edge of the wire array is at $x = 0$ mm. (b) Magnetic field 397 ns after current start. The region sampled by the lineout in Fig. 3 is shown.

[34]. An electron density map in the x - z plane is shown in Fig. 2(a). The observed shock structure comprises two distinct types of shock. A subcritical shock spans the region upstream of both obstacles. This shock is smooth and continuous between the obstacles and forms as a single shock ~ 300 ns after current start at a distance $\sim d_i$ from the obstacles. The formation process of similar shocks is studied in Refs. [30,32]; here we study the shocks later in time during a quasi-steady state phase. In addition to the subcritical shock, two secondary shocks, referred to here as stagnation shocks, form closer to the obstacles, downstream of the subcritical shock. These do not propagate upstream to reach the position of the subcritical shock, and have an abrupt density increase.

The magnetic field distribution in the x - z plane was measured using Faraday rotation imaging [34]. Fig. 2(b) shows the measured magnetic field. In the region between the obstacles, the magnetic field increases from 1.5–2 T upstream of the subcritical shock to 3–4 T in the downstream, showing that magnetic field is compressed across the shock. Redistribution of the laser intensity caused by refraction at density gradients (shadowgraphy) leads to an intensity modulation at the subcritical shock ramp so magnetic field cannot be inferred inside the subcritical shock.

Optical Thomson Scattering (TS) of the ion acoustic feature provided localized measurements of plasma velocity and temperatures at 14 localized plasma volumes [shown in Fig. 2(a)] [34,44,45]. The flow velocity directly upstream of the subcritical shock was 45 km s^{-1} ($KE_{\text{ion}} \sim 290 \text{ eV}$), and the temperature was $T_e = T_i = 12 \pm 3 \text{ eV}$.

A combined analysis of interferometry, Faraday rotation, and TS data allows characteristic dimensionless parameters of the upstream plasma to be evaluated; see Table I. The thermal and magnetic pressures differ by less than a factor of 2, while the ram pressure is substantially larger. The Mach numbers all exceed unity, so the flow will form a shock when colliding with stationary obstacles. The critical Mach number (which depends on β_{th} and the shock angle)

TABLE I. Characteristic plasma parameters upstream of the subcritical shock ~ 400 ns after current start (details in the Supplemental Material [34]). To evaluate the magnetic Reynolds number, a scale length of 10 mm, the distance between the wire array and the obstacles, gives $Re_M \sim 10$ while a distance of ~ 0.8 mm, the subcritical shock width, gives $Re_M \sim 1$.

Dimensionless parameter		Value
Thermal beta	β_{th}	1.7
Dynamic beta	β_{ram}	18
Sonic Mach number	M_S	2.5
Alfvénic Mach number	M_A	3
Magnetosonic Mach number	M_{MS}	1.9
Reynolds number	Re	4×10^4
Magnetic Reynolds number	Re_M	$10 \rightarrow 1$

for these upstream parameters is $M_C \sim 1.4$ (Fig. 4 in Ref. [46]). $M_{MS} \sim 1.9 > 1.4$ suggests that the flow is supercritical; however, we note that only a small increase in magnetic field, to 2.2 T, would result in $\beta_{th} = 1$ and $M_{MS} \sim M_C \sim 1.7$. Since the magnetic field inferred from the Faraday rotation data is a lower bound for $B_y(y = 0 \text{ mm})$ [34], we conclude that a subcritical shock may form. The large Reynolds number means viscous dissipation will occur on scales much smaller than the system size. However, the modest value of Re_M shows that while magnetic field is expected to be advected in the upstream, magnetic diffusion will become important on the spatial scale of the shocks.

Figs. 3(a) and 3(b) show the velocity and temperature measurements from TS in the $z = 0$ mm plane alongside lineouts of electron density and magnetic field [the locations of the TS scattering volumes are shown in Fig. 2(a)]. The electron density increases across the subcritical shock before decreasing as the plasma expands into the vacuum behind the shock. The velocity, which was measured locally, is consistent with 1D conservation of mass, suggesting that line integration does not affect the interferometry result. The ion and electron temperatures are equal across the shock and change by less than 10 eV [$T = T_e = T_i$ is presented in Fig. 3(b)].

To show that the shock is subcritical (and is a shock), we must show that the flow remains supersonic (but becomes submagnetosonic) across the shock. The sound speed, Alfvén speed, and fast-magnetosonic speed are compared with the flow velocity in Fig. 3(c). The flow becomes submagnetosonic across the shock but remains supersonic, a defining feature of subcritical shocks. As the flow passes the obstacles, it expands into the vacuum and becomes supermagnetosonic again.

We characterize the subcritical shock in terms of the density compression ratio and the shock width. The compression ratio R is estimated from electron density measurements. The compression ratio is estimated by comparing the downstream density in experiments with

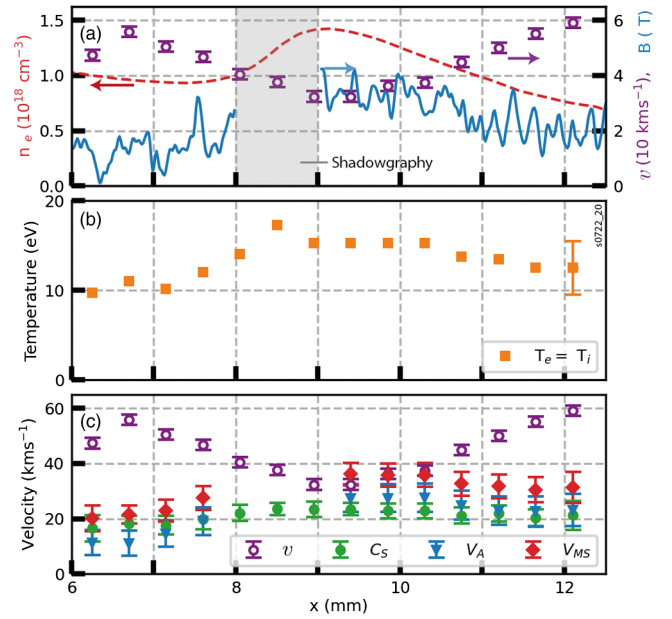


FIG. 3. Thomson scattering data and plasma parameter profiles. (a) Flow velocity at 416 ns with electron density and magnetic field lineouts at $z = 0$ mm. The region in which the magnetic field measurement was affected by shadowgraphy is shaded. (b) Temperature at $z = 0$ mm. A characteristic error bar which includes modeling uncertainty is shown for the final data point (we expect this to be mostly systematic). (c) Velocity compared with the sound speed C_S , Alfvén speed V_A , and fast-magnetosonic speed V_{MS} across the subcritical shock. Values which depend on B are excluded for $x = 8-9$ mm where Faraday rotation measurements are affected by shadowgraphy.

obstacles to the density at the same x location in an experiment without obstacles (null shot), which yields $R = 2.7 \pm 0.8$. This is consistent with the MHD shock jump conditions [Eq. (6) in [47]]. The measured shock width, defined as the distance between 10 and 90% of the density jump, was 0.87 ± 0.08 mm. The width of a shock is determined by the dissipative and/or dispersive processes which increase entropy and transport energy at the shock front [48]. Table II shows a comparison of the shock width with characteristic length scales for viscous dissipation ($\lambda_{i,i}$), Ohmic dissipation (L_η), electron heat conduction (L_χ), and the formation of a cross shock potential due to two-fluid effects (d_i).

The ion-ion mean free path is ~ 4 orders of magnitude smaller than the shock width. This indicates that viscous dissipation does not shape the shock, as expected for a subcritical shock. Resistive diffusion, heat conduction, and two-fluid effects may all contribute to the shaping of a subcritical shock, and their characteristic scale lengths are all comparable to the shock width. The largest dissipative scale, and the scale closest to the shock width is L_η . This suggests that Ohmic dissipation plays the most significant role in shock shaping. Since L_η is approximately equal to the shock width, the shock structure can be described by

TABLE II. Comparison of the measured shock width with characteristic dissipative and dispersive scale lengths [34].

Parameter		Value (mm)
Shock width		0.87 ± 0.08
Ion-ion mfp	$\lambda_{i,i}$	8×10^{-5}
Resistive diffusion length	L_η	0.75
Electron thermal diffusion length	L_χ	0.16
Ion inertial length	d_i	0.69

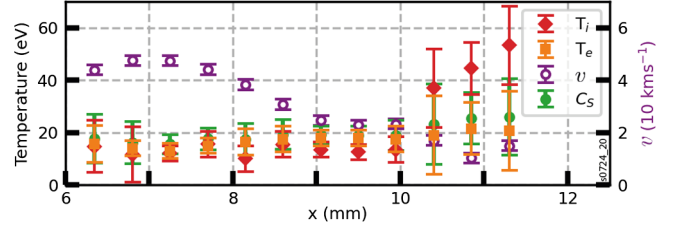
classical (Spitzer) resistive MHD only, without including anomalous resistivity. The contribution of electron heat conduction to shock shaping will be less than that of Ohmic dissipation since $L_\eta \sim 5 \times L_\chi$ in the upstream and $L_\eta > L_\chi$ across the entire subcritical shock. Two-fluid effects may also contribute to shock structure since d_i is also approximately equal to the shock width. The formation of a cross shock potential due to two-fluid separation is a dispersive effect and does not dissipate kinetic energy. Rather, it excites whistler waves which carry energy away from the shock front. Since the dispersive scale d_i is approximately equal to the largest dissipative scale L_η , this energy will be quickly dissipated and will not result in oscillations typical of collisionless shock structures. We note that while heat conduction and two-fluid effects may well contribute to shock structure, resistive diffusion alone is sufficient to explain the observed shock width.

Since viscous dissipation does not shape the subcritical shock, the main heating mechanisms will be adiabatic and Ohmic. We estimate the heating due to adiabatic compression by calculating $T_2 = T_1 \times R^{\gamma-1} = 23 \pm 3$ eV for $\gamma = 5/3$. Ohmic heating will also increase the temperature, and the heating power per unit volume can be estimated by

$$P = \eta J^2 = \eta \left(\frac{c}{4\pi} \right)^2 |\nabla \times B|^2, \quad (1)$$

where η is the Spitzer resistivity and $\nabla \times B \approx \Delta B_y / \Delta x \approx 2$ T/1 mm. This yields an increase in electron temperature of ~ 20 eV at the subcritical shock (assuming a velocity of 40 km s $^{-1}$). However, we note that the radiative cooling time (~ 10 ns [34,49]) is less than the time the plasma takes to cross the shock (~ 25 ns) so radiative cooling will reduce the observed temperature change. The estimated heating rate due to compression and Ohmic heating is ~ 40 eV/25 ns = 1.6 eV ns $^{-1}$. Balancing this against the radiative cooling rates presented in Ref. [49] requires an electron temperature of ~ 15 eV, in good agreement with the experimental results.

Behind the subcritical shock, the stagnation shock wings are stationary and remain downstream of the subcritical shock for the duration of the experiment. This suggests that the relevant Mach number for the stagnation shocks is M_S , since this remains greater than unity across the subcritical


 FIG. 4. Ion temperature, electron temperatures, velocity, and C_s at $z = -2$ mm.

shock. In this case, the stagnation shocks should be hydrodynamic jumps, formed by viscous dissipation on a spatial scale comparable to $\lambda_{i,i}$. This is below the resolution of the interferometry diagnostic (~ 0.05 mm), but TS measurements provide strong evidence for this interpretation. Figure 4 shows TS temperature measurements collected in the $x - y$ plane at $z = -2$ mm which cross a stagnation shock [see locations of scattering volumes in Fig. 2(a)]. The measurements are consistent with those at $z = 0$ mm in the upstream and subcritical shock (see Fig. 3), but show substantial ion heating to 40–70 eV at the stagnation shock. The flow velocity decreases to ~ 10 km s $^{-1}$ in this region and becomes subsonic. Both the ion heating and the subsonic downstream flow indicate that, in contrast to the subcritical shock, viscous dissipation of kinetic energy into ion thermal energy shapes the stagnation shocks. The observation of hydrodynamic shocks in the downstream of a subcritical shock is novel and was not discussed in the theory. We are, as yet, unsure if this is unique to collisional plasmas, where $\lambda_{i,i} \ll L_\eta$ or whether such phenomena may also occur in collisionless plasmas.

To further investigate the shaping of subcritical shocks, 2D simulations were carried out using the Gorgon MHD code [50,51]. The code uses magnetized resistivity and thermal conductivity coefficients based on the Epperlein-Haines model [13] and implements an optically thin radiative recombination model. A plasma flow was injected from the left hand boundary at a rate determined by the ablation rocket model [52] and was then accelerated by the experimentally measured current waveform. The ablation velocity used to determine the mass injection rate was adjusted so that the parameters directly upstream of the shock matched the experiment. The magnetic field at the injection point was then adjusted until the location of the shock at 400 ns matched the experiment.

Reasonable agreement with the experimental result was found with a width of 1.0 mm and $L_{\eta,\text{sim}} = 0.66$ mm, so $\text{width}_{\text{sim}} = 1.5 \times L_{\eta,\text{sim}}$. However, a larger magnetic field than in the experiment was required to achieve the correct shock location in the simulation. With all other parameters matched, a field of 4.8 T, compared with 1.5–2 T in the experiment, was needed. Figure 5 compares the 4.8 T case with a simulation in which we also match the experimental

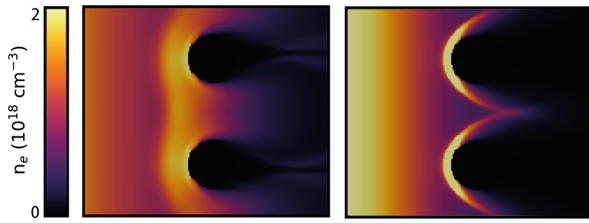


FIG. 5. Simulation results at 400 ns. (a) Matched shock position with $B_u = 4.8$ T. (b) Matched B_u .

B field. The morphology of the shock is clearly not matched in Fig. 5(b). A shock reflection appears to form, and the absence of a normal shock between the obstacles makes measuring the shock width difficult. The fact that a larger field is required to match the shock morphology is discussed in detail in the Appendix. We note here that L_η does not depend on B and that B was adjusted to match the shock position, not its width. Therefore, the discrepancy should not affect our conclusion that the simulations support our experimental finding that the shock width is approximately equal to the resistive diffusion length.

In summary, we have presented an investigation of perpendicular subcritical shocks in a collisional plasma with $M_{MS} \sim 1.9$ and $\lambda_{i,i} \ll L_\eta$. We demonstrate that the shock is subcritical by showing that $M_S > 1$ across the shock. We confirm the theoretically predicted absence of a hydrodynamic jump, and show that the shock width is approximately equal to the classical (Spitzer) resistive diffusion length. We observe little heating at the subcritical shock, which is consistent with an absence of viscous dissipation. In contrast, downstream stagnation shocks cause substantial ion heating and produce a subsonic downstream flow. We interpret these shocks to be hydrodynamic in nature. Two-dimensional resistive MHD simulations reproduce the experimentally observed morphology of the subcritical shock and demonstrate that Ohmic dissipation sets the shock width, which is comparable to the classical resistive diffusion length.

We thank Drs. E. Yu and D. Ho for useful discussion. This work was supported by First Light Fusion Ltd. and by the US Department of Energy (DOE), including Awards No. DE-NA0003764 and No. DE-SC0020434.

Appendix on the differences between experiments and simulations.—Two-dimensional resistive MHD simulations were able to reproduce the observed width of the subcritical shock. However, we have found that a larger than expected magnetic field was required to match the shock morphology and position (having a density peak at 9 mm at 400 ns). This discrepancy was also observed in 2D MHD simulations using the *AstroBEAR* code [53,54]. Here we discuss the reason for this discrepancy and the potential consequences for our conclusions. Figure 6 compares the simulation at 400 ns with the experimental data presented

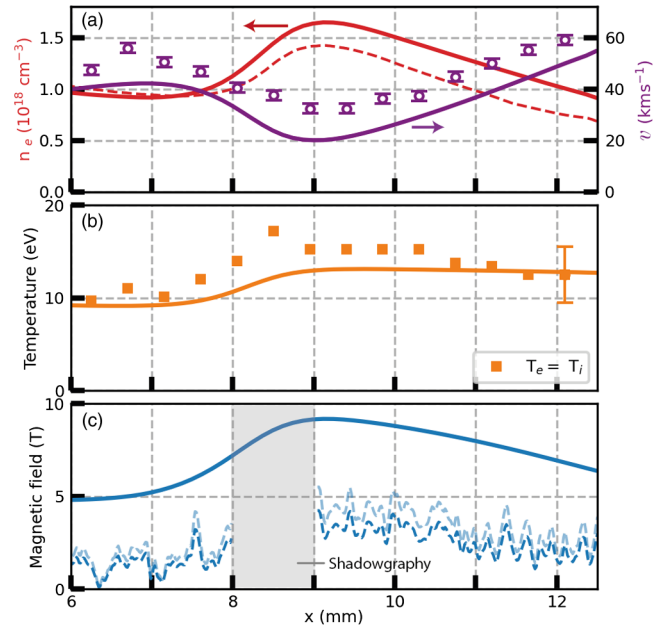


FIG. 6. Comparison of simulated parameters, in the midplane between the obstacles, at 400 ns (solid lines) with the experimental parameters presented in Fig. 3 (data points and dashed lines). The light blue dashed line shows the experimental B field scaled up by a factor of 1.3, the maximum systematic error attributable to line integration effects in the Faraday rotation data.

in Fig. 3. Good agreement with the experimental electron density, velocity, and temperature was achieved. However, there is a significant difference between the measured and simulated magnetic field.

We do not believe it is possible that the magnetic field in the experiment is as large as the simulation suggests. Firstly, a field this large would mean the experimental system was no longer in pressure balance. In the shock frame, the upstream and downstream total pressures should balance. This is true for the experimentally measured field, but not true if the simulation field is used. In the simulation, the total pressure is balanced in the shock frame because the shock has a much larger velocity in the lab frame. This is discussed further below.

Secondly, we have estimated the extent to which Faraday rotation polarimetry underestimates $B_y(y = 0 \text{ mm})$ [34]. We have carried out a 3D MHD simulation of the wire array and obstacles using the *Gorgon* code. The simulation did not reproduce the observed subcritical shock (unsurprisingly given our 2D results), and we do not show it here. Nevertheless, the 3D simulation was useful since it showed that a line integrated measurement would not underestimate B_y by more than a factor of 1.3, at any distance from the wire array. Multiplying the experimentally measured magnetic field by 1.3 would give an upstream magnetic field of 2–2.6 T (rather than 1.5–2 T). This is well below the 4.8 T seen in the simulation (see Fig. 6), but is consistent with the 2.2 T required to agree with theory (see discussion in the main text).

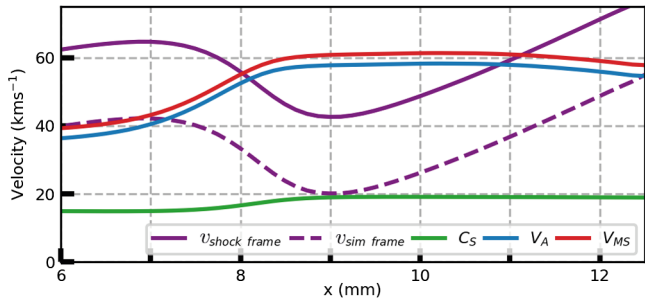


FIG. 7. Comparison of the flow velocity with C_S , V_A , and V_{MS} . The velocity in the simulation frame is dashed, and the velocity in the shock frame is solid ($v_{\text{shock}} = v_{\text{sim}} + 22.5 \text{ km s}^{-1}$ at 400 ns). To determine the type of shock, v_{shock} should be used.

Given the discrepancy in the magnetic field, it is important to show that the shock in the simulation is also subcritical. As with the experiment, we do this by comparing the flow velocity with C_S , V_A , and V_{MS} in Fig. 7. In contrast to the experiment, where the shock is approximately stationary, the shock in the simulation moves away from the obstacles at 22.5 km s^{-1} (see Fig. 8 and discussion below). It is clear that the shock is subcritical in the shock frame, so the physics responsible for the shock structure should be the same as in the experiment.

A good candidate to explain the discrepancy between the experiment and simulations is two-fluid effects, which are not accounted for in the simulations. In the experiment, the subcritical shock started to form at approximately d_i from the obstacles, 300 ns after current start. Burdiak *et al.* [30] studied the formation of similar shocks to ours and concluded that at early time $d_i \gg L_\eta$, so the shock formation should be governed by two-fluid physics [see Fig. 10(b) in [30]]. This may have the effect of setting up a shock at a larger distance from the obstacles, which is then sustained by resistive diffusion when $d_i < L_\eta$ (after about 300 ns). In this case, since the simulations cannot reproduce two-fluid effects, a larger magnetic field is required to push the subcritical shock to the location which we observe in the experiment.

Tracking the evolution of the subcritical shock position provides strong evidence for this interpretation (Fig. 8). In the experiment, the shock was first observed at around 300 ns after the current start and then remained approximately stationary in the laboratory frame. In the simulation, the shock formed much earlier and much further from the wire array because the simulation does not include two-fluid effects and L_η is small at early times. In order to match the experimental position of the shock at 400 ns, a larger magnetic field was required. However, this additional magnetic pressure meant the shock continued to move forward at 22.5 km s^{-1} at 400 ns.

The result is that by using an increased magnetic field to account for the absence of two-fluid physics in the simulation, we have been able to match the majority of

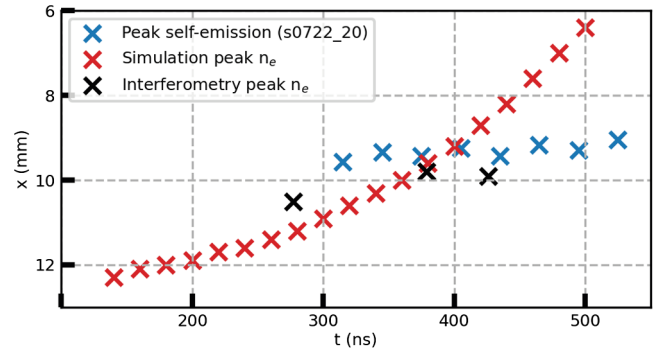


FIG. 8. Position vs time data at $z = 0 \text{ mm}$ (the midplane). The maximum electron density in the simulation is compared with the maximum experimental electron density (from different shots) and the peak optical self-emission intensity (from a single shot). Optical self-emission images were recorded with a 30 ns inter-frame spacing and a 5 ns exposure along the same line of sight as the interferometry. In this experimental regime where the temperature is relatively constant, the optical self-emission intensity is well correlated with electron density.

the experimental parameters at a fixed time, but have been unable to match the evolution of the shock position. Extended MHD, which is under development in a number of codes, may resolve this issue, but this would be a substantial project and is beyond the scope of this work.

As we have shown, there are some limitations to using an MHD code to simulate our experiment. However, the Gorgon code is widely used and well benchmarked for studying highly collisional plasmas [55]. Since L_η does not depend on B , and $L_\eta > d_i$ by 400 ns, our conclusion that the simulations support our experimental evidence seems to be robust. These are that a subcritical shock is formed, that there is no isomagnetic jump, and that the shock width is approximately equal to the resistive diffusion length.

*daniel.russell13@imperial.ac.uk

- [1] R. A. Treumann, Fundamentals of collisionless shocks for astrophysical application, 1. Non-relativistic shocks, *Astron. Astrophys. Rev.* **17**, 409 (2009).
- [2] F. D. Hoffmann and E. Teller, Magneto-hydrodynamic shocks, *Phys. Rev.* **80**, 692 (1950).
- [3] P. Germain, Shock waves and shock-wave structure in magneto-fluid dynamics, *Rev. Mod. Phys.* **32**, 951 (1960).
- [4] R. V. Polovin, Shock waves in magnetohydrodynamics, *Sov. Phys. Usp.* **3**, 677 (1961).
- [5] J. E. Anderson, *Magnetohydrodynamic Shock Waves* (MIT Press, Cambridge, MA, 1963).
- [6] W. Marshall, The structure of magneto-hydrodynamic shock waves, *Proc. R. Soc. A* **233**, 367 (1955).
- [7] F. V. Coroniti, Dissipation discontinuities in hydromagnetic shock waves, *J. Plasma Phys.* **4**, 265 (1970).
- [8] D. J. Mullan, The structure of transverse hydromagnetic shocks in regions of low ionization, *Mon. Not. R. Astron. Soc.* **153**, 145 (1971).

- [9] B. T. Draine, Interstellar shock waves with magnetic precursors, *Astrophys. J.* **241**, 1021 (1980).
- [10] M. M. Mellott and E. W. Greenstadt, The structure of oblique subcritical bow shocks: ISEE 1 and 2 observations, *J. Geophys. Res.* **89**, 2151 (1984).
- [11] D. B. Schaeffer, E. T. Everson, A. S. Bondarenko, S. E. Clark, C. G. Constantin, D. Winske, W. Gekelman, and C. Niemann, Experimental study of subcritical laboratory magnetized collisionless shocks using a laser-driven magnetic piston, *Phys. Plasmas* **22**, 113101 (2015).
- [12] S. I. Braginskii, Transport processes in a plasma, *Rev. Plasma Phys.* **1**, 205 (1965).
- [13] E. M. Epperlein and M. G. Haines, Plasma transport coefficients in a magnetic field by direct numerical solution of the Fokker-Planck equation, *Phys. Fluids* **29**, 1029 (1986).
- [14] J. D. Sadler, C. A. Walsh, and H. Li, Symmetric Set of Transport Coefficients for Collisional Magnetized Plasma, *Phys. Rev. Lett.* **126**, 075001 (2021).
- [15] J. R. Davies, H. Wen, J. Y. Ji, and E. D. Held, Transport coefficients for magnetic-field evolution in inviscid magnetohydrodynamics, *Phys. Plasmas* **28**, 012305 (2021).
- [16] J. Hamilton and C. E. Seyler, Formulation of 8-moment plasma transport with application to the nerst effect, *Phys. Plasmas* **28**, 022306 (2021).
- [17] A. N. Simakov, Electron transport in a collisional plasma with multiple ion species in the presence of a magnetic field, *Phys. Plasmas* **29**, 022304 (2022).
- [18] G. A. Wurden, S. C. Hsu, T. P. Intrator, T. C. Grabowski, J. H. Degnan, M. Domonkos, P. J. Turchi, E. M. Campbell, D. B. Sinars, M. C. Herrmann, R. Betti, B. S. Bauer, I. R. Lindemuth, R. E. Siemon, R. L. Miller, M. Laberge, and M. Delage, Magneto-inertial fusion, *J. Fusion Energy* **35**, 69 (2016).
- [19] S. A. Slutz, M. C. Herrmann, R. A. Vesey, A. B. Sefkow, D. B. Sinars, D. C. Rovang, K. J. Peterson, and M. E. Cuneo, Pulsed-power-driven cylindrical liner implosions of laser preheated fuel magnetized with an axial field, *Phys. Plasmas* **17**, 056303 (2010).
- [20] M. R. Gomez *et al.*, Performance Scaling in Magnetized Liner Inertial Fusion Experiments, *Phys. Rev. Lett.* **125**, 155002 (2020).
- [21] L. J. Perkins, D. D.-M. Ho, B. G. Logan, G. B. Zimmerman, M. A. Rhodes, D. J. Strozzi, D. T. Blackfield, and S. A. Hawkins, The potential of imposed magnetic fields for enhancing ignition probability and fusion energy yield in indirect-drive inertial confinement fusion, *Phys. Plasmas* **24**, 062708 (2017).
- [22] D. B. Sinars, Review of pulsed power-driven high energy density physics research on Z at Sandia, *Phys. Plasmas* **27**, 070501 (2020).
- [23] R. Hua, J. Kim, M. Sherlock, M. Bailly-Grandvaux, F. N. Beg, C. McGuffey, S. Wilks, H. Wen, A. Joglekar, W. Mori, and Y. Ping, Self-Generated Magnetic and Electric Fields at a Mach-6 Shock Front in a Low Density Helium Gas by Dual-Angle Proton Radiography, *Phys. Rev. Lett.* **123**, 215001 (2019).
- [24] J. D. Moody *et al.*, Progress on the magnetized ignition experimental platform for the national ignition facility, *Bull. Am. Phys. Soc.* **2021**, UO04.007 (2021).
- [25] D. Ho, G. Zimmerman, A. Velikovich, R. Kulsrud, J. Moody, J. Harte, and A. Kritcher, Magnetized ICF: Role of e-thermal conductivity on imploding shock and high-yield capsule designs, *Bull. Am. Phys. Soc.*, **2021**, UO04.010 (2021).
- [26] C. A. Walsh, S. O'Neill, J. P. Chittenden, A. J. Crilly, B. Appelbe, D. J. Strozzi, D. Ho, H. Sio, B. Pollock, L. Divol, E. Hartouni, M. Rosen, B. G. Logan, and J. D. Moody, Magnetized ICF implosions: Scaling of temperature and yield enhancement, *Phys. Plasmas* **29**, 042701 (2022).
- [27] C. F. Kennel, Shock structure in classical magnetohydrodynamics, *J. Geophys. Res.* **93**, 8545 (1988).
- [28] M. A. Liberman and A. L. Velikovich, *Physics of Shock Waves in Gases and Plasmas* (Springer-Verlag, Berlin, 1986).
- [29] A. J. Harvey-Thompson, S. V. Lebedev, S. N. Bland, J. P. Chittenden, G. N. Hall, A. Marocchino, F. Suzuki-Vidal, S. C. Bott, J. B. Palmer, and C. Ning, Quantitative analysis of plasma ablation using inverse wire array z pinches, *Phys. Plasmas* **16**, 022701 (2009).
- [30] G. C. Burdiak, S. V. Lebedev, S. N. Bland, T. Clayson, J. Hare, L. Suttle, F. Suzuki-Vidal, D. C. Garcia, J. P. Chittenden, S. Bott-Suzuki, A. Ciardi, A. Frank, and T. S. Lane, The structure of bow shocks formed by the interaction of pulsed-power driven magnetised plasma flows with conducting obstacles, *Phys. Plasmas* **24**, 072713 (2017).
- [31] I. H. Mitchell, J. M. Bayley, J. P. Chittenden, J. F. Worley, A. E. Dangor, M. G. Haines, and P. Choi, A high impedance mega-ampere generator for fiber z-pinch experiments, *Rev. Sci. Instrum.* **67**, 1533 (1996).
- [32] S. V. Lebedev *et al.*, The formation of reverse shocks in magnetized high energy density supersonic plasma flows, *Phys. Plasmas* **21**, 056305 (2014).
- [33] J. P. Chittenden, S. V. Lebedev, B. V. Oliver, E. P. Yu, and M. E. Cuneo, Equilibrium flow structures and scaling of implosion trajectories in wire array Z pinches, *Phys. Plasmas* **11**, 1118 (2004).
- [34] See Supplemental Material at <http://link.aps.org/supplemental/10.1103/PhysRevLett.129.225001> for the calculations used in Tables I and II, details of the radiative cooling model and details of the diagnostic methods, which includes Refs. [35–43].
- [35] D. D. Ryutov, R. P. Drake, J. Kane, E. Liang, B. A. Remington, and W. M. Wood-Vasey, Similarity criteria for the laboratory simulation of supernova hydrodynamics, *Astrophys. J.* **518**, 821 (1999).
- [36] J. Huba, *NRL Plasma Formulary* (Naval Research Laboratory, Washington DC, 2013).
- [37] R. S. Sutherland and M. A. Dopita, Cooling functions for low-density astrophysical plasmas, *Astrophys. J. Suppl. Ser.* **88**, 253 (1993).
- [38] G. Espinosa, J. M. Gil, R. Rodriguez, J. G. Rubiano, M. A. Mendoza, P. Martel, E. Minguez, F. Suzuki-Vidal, S. V. Lebedev, G. F. Swadling, G. Burdiak, L. A. Pickworth, and J. Skidmore, Collisional-radiative simulations of a supersonic and radiatively cooled aluminum plasma jet, *High Energy Density Phys.* **17**, 74 (2015).
- [39] J. D. Hare, J. MacDonald, S. N. Bland, J. Dranczewski, J. W. D. Halliday, S. V. Lebedev, L. G. Suttle, E. R. Tubman,

- and W. Rozmus, Two-colour interferometry and Thomson scattering measurements of a plasma gun, *Plasma Phys. Controlled Fusion* **61**, 085012 (2019).
- [40] D. R. Russell, Bow shock interaction experiments in a magnetised collisional plasma, Ph. D. thesis, Imperial College London, 2021, [10.25560/92937](https://doi.org/10.25560/92937).
- [41] D. H. Froula, S. H. Glenzer, N. C. Luhmann, Jr., and J. Sheffield, *Plasma Scattering of Electromagnetic Radiation: Theory and Measurement Techniques*, 2nd ed. (Academic Press, New York, 2011).
- [42] J. D. Hare, High energy density magnetic reconnection experiments in colliding carbon plasma flows, Ph.D. thesis, Imperial College London, 2017, [10.25560/49251](https://doi.org/10.25560/49251).
- [43] N.-P. L. Niasse, Development of a pseudo non-LTE model for Z-pinch simulations, Ph.D. thesis, Imperial College London, 2011, [10.25560/9324](https://doi.org/10.25560/9324).
- [44] G. F. Swadling, S. V. Lebedev, G. N. Hall, S. Patankar, N. H. Stewart, R. A. Smith, A. J. Harvey-Thompson, G. C. Burdiak, P. D. Grouchy, J. Skidmore, L. Suttle, F. Suzuki-Vidal, S. N. Bland, K. H. Kwek, L. Pickworth, M. Bennett, J. D. Hare, W. Rozmus, and J. Yuan, Diagnosing collisions of magnetized, high energy density plasma flows using a combination of collective Thomson scattering, Faraday rotation, and interferometry (invited), *Rev. Sci. Instrum.* **85**, 11E502 (2014).
- [45] L. G. Suttle, J. D. Hare, J. W. Halliday, S. Merlini, D. R. Russell, E. R. Tubman, V. Valenzuela-Villaseca, W. Rozmus, C. Bruulsema, and S. V. Lebedev, Collective optical Thomson scattering in pulsed-power driven high energy density physics experiments (invited), *Rev. Sci. Instrum.* **92**, 033542 (2021).
- [46] J. P. Edmiston and C. F. Kennel, A parametric survey of the first critical Mach number for a fast MHD shock, *J. Plasma Phys.* **32**, 429 (1984).
- [47] P. Hartigan, Shock waves in outflows from young stars, *Astrophys. Space Sci.* **287**, 111 (2003).
- [48] C. F. Kennel, J. P. Edmiston, and T. Hada, A quarter century of collisionless shock research, in *Collisionless Shocks in the Heliosphere: A Tutorial Review* (American Geophysical Union (AGU), Washington, DC, 1985), pp. 1–36, [10.1029/GM034p0001](https://doi.org/10.1029/GM034p0001).
- [49] F. Suzuki-Vidal, S. V. Lebedev, A. Ciardi, L. A. Pickworth, R. Rodriguez, J. M. Gil, G. Espinosa, P. Hartigan, G. F. Swadling, J. Skidmore, G. N. Hall, M. Bennett, S. N. Bland, G. Burdiak, P. D. Grouchy, J. Music, L. Suttle, E. Hansen, and A. Frank, Bow shock fragmentation driven by a thermal instability in laboratory astrophysics experiments, *Astrophys. J.* **815**, 96 (2015).
- [50] J. P. Chittenden, S. V. Lebedev, C. A. Jennings, S. N. Bland, and A. Ciardi, X-ray generation mechanisms in three-dimensional simulations of wire array Z-pinches, *Plasma Phys. Controlled Fusion* **46**, B457 (2004).
- [51] A. Ciardi, S. V. Lebedev, A. Frank, E. G. Blackman, J. P. Chittenden, C. J. Jennings, D. J. Ampleford, S. N. Bland, S. C. Bott, J. Rapley, G. N. Hall, F. A. Suzuki-Vidal, A. Marocchino, T. Lery, and C. Stehle, The evolution of magnetic tower jets in the laboratory, *Phys. Plasmas* **14**, 056501 (2007).
- [52] S. V. Lebedev, F. N. Beg, S. N. Bland, J. P. Chittenden, A. E. Dangor, M. G. Haines, K. H. Kwek, S. A. Pikuz, and T. A. Shelkovenko, Effect of discrete wires on the implosion dynamics of wire array Z pinches, *Phys. Plasmas* **8**, 3734 (2001).
- [53] A. J. Cunningham, A. Frank, P. Varnière, S. Mitran, and T. W. Jones, Simulating magnetohydrodynamical flow with constrained transport and adaptive mesh refinement: Algorithms and tests of the AstroBEAR code, *Astrophys. J. Suppl. Ser.* **182**, 519 (2009).
- [54] J. J. Carroll-Nellenback, B. Shroyer, A. Frank, and C. Ding, Efficient parallelization for amr mhd multiphysics calculations; implementation in astrobear, *J. Comput. Phys.* **236**, 461 (2013).
- [55] G. F. Swadling, S. V. Lebedev, N. Niasse, J. P. Chittenden, G. N. Hall, F. Suzuki-Vidal, G. Burdiak, A. J. Harvey-Thompson, S. N. Bland, P. D. Grouchy, E. Khoory, L. Pickworth, J. Skidmore, and L. Suttle, Oblique shock structures formed during the ablation phase of aluminium wire array Z-pinches, *Phys. Plasmas* **20**, 022705 (2013).